Mechanically-Excited Multicolor Luminescence in Lanthanide Ions

Yangyang Du, Yue Jiang, Tianying Sun, Jianxiong Zhao, Bolong Huang, Dengfeng Peng*, and Feng Wang**

Y. Du, Dr. T. Sun, J. Zhao, Prof. F. Wang

Department of Materials Science and Engineering,

City University of Hong Kong, 83 Tat Chee Avenue, Hong Kong SAR, China

E-mail: fwang24@cityu.edu.hk

Y. Jiang, Prof. D. Peng

College of Optoelectronic Engineering, Shenzhen University, Shenzhen 518060, China

E-mail: pengdengfeng@szu.edu.cn

Prof. B. Huang

Department of Applied Biology and Chemical Technology, The Hong Kong Polytechnic University, Hung Hom, Kowloon, Hong Kong SAR, China

E-mail: bhuang@polyu.edu.hk

Y. Du, Dr. T. Sun, J. Zhao, Prof. F. Wang

City Universities of Hong Kong Shenzhen Research Institute, Shenzhen 518057, China

Keywords: Mechanoluminescence, Lanthanide, CaZnOS, Multicolor tuning, Optical coding

Abstract: Mechanoluminescence (ML) featuring photon emission by mechanical stimuli is promising for applications such as stress sensing, display, and artificial skin. However, the progress of utilizing ML processes has been constrained by the limited range of available ML emission spectra. Herein, we report a general strategy for expanding the emission of ML through the use of lanthanide emitters. We developed a lithium-assisted annealing method for effective incorporation of various lanthanide ions (e.g.; Tb^{3+}, Eu^{3+}, Pr^{3+}, Sm^{3+}, Er^{3+}, Dy^{3+}, Ho^{3+}, Nd^{3+}, Tm^{3+}, and Yb^{3+}) into CaZnOS crystals that are identified as one of the most efficient host materials for ML. These doped CaZnOS crystals show efficient and tunable ML spanning full spectrum from violet to near infrared. The multicolor ML materials were used to create

encrypted anti-counterfeiting patterns, which produce spatially resolvable optical codes under single-point dynamic pressure of a ball-point pen.

Introduction:

Mechanoluminescent materials capable of emitting visible light under mechanical stimuli are of significant technological importance. These materials are potentially useful for constructing optoelectrical devices that requires no optical or electrical sources of energy for their operation[1]. Recent studies by several independent groups have substantiated the unique role of ML in moden technologies such as wind-driven dispaly, optical sensor, and artificial skin[2]. However, practical application of these systems is hindered by limited range of available ML emission colors. Therefore, development of multicolor ML materials displaying high and equal brightness across the whole spectral range is one of the most urget task in ML research.

Since the discovery of ML in 1605[1], continuous efforts have been devoted to the search for new ML materails and a large diversity of compounds have been found to show ML[3]. Nethetheless, only very few material systems known to date can produce sufficiently bright and self-recoverable ML to satisfy technological applications. Efficient ML materails are typically composed of piezoelectric materials such as ZnS, CaZnOS, and $LiNbO_3$, which promote the formation of lattice-defect complexes by strain-induced piezoelectric potential due to strong electron-lattice coupling[4]. These lattice-defect complexes function as active energy carriers and migration centers in ML processes[5]. In addition, substitutional dopant ions are usually needed to promote the stress-to-photon conversion processes. Dopant ions are able to capture strain-

induced energies associated with lattice defects, and subsequently produce photon emissions at high effciencies. Dopant ions also introduce additional energy levels to tune the emission profiles[6]. The most commonly used dopant ion is Mn^{2+} that substitutes for Zn^{2+} in the host materials. Due to their close chemical properties, Mn^{2+} can be convienent incorporated into the host lattice at high concentrations without deleterious effects[7].

Attempts have also been made to activate ML materials with lanthanide dopants that comprise a familiy of chemically similar elements[8]. Although lanthanides are very successful as luminescent dopants in insulators, their use in ML have been met with limited success because the low compabilbity between lanthanide dopants and semiconducting ML host materials. Activation of ML materials with lanthanide ions requires careful control of host/dopant combination, dopant concentration, and method of preparation. Lanthanide-doped inorganic ML materials in literatures typically comprise low concentrations of Sm^{3+} (1 mol%), Er^{3+} (0.5 mol%), and Nd^{3+} (2 mol%) activitors[9], which render limited emission colors and relatively low ML emission intensities. Particularly, no approach is available to achieve ML in Tb^{3+} dopants that is known as the most efficient lanthanide emitter in the visible spectral range.

In this paper, we develop a general method to incorporate various lanthanide (e.g. Tb^{3+}, Eu^{3+}, Pr^{3+}, Sm^{3+}, Er^{3+}, Dy^{3+} Ho^{3+}, Nd^{3+}, and Yb^{3+}) ions into CaZnOS for creating multicolor ML emissions by mechanical excitations. We demonstrate effective lanthanide doping (> 3 mol%) by a Li-assisted solid state reaction. We show bright multicolor ML emission from these doped CaZnOS phosphors with an intensity comparable to that of the classical CaZnOS:Mn. We also establish an approach to fine-tuning the ML emission colors from green to red by combining

Tb^{3+}- and Mn^{2+}-doped CaZnOS phosphors. Our results indicate that the multicolor ML phosphors can be used to create optically encoded graphics for anti-counterfeiting applications.

Results and discussions:

CaZnOS was chosen as the host materials in our study owing to its ability to render efficient ML and the convenience for impurity doping. The CaZnOS host contains two types of cation sites, namely Zn^{2+} (CN4, 0.60Å) and Ca^{2+} (CN6, 1.00Å) (**Figure 1a**)[7], which are able to accommodate transition metal ions (e.g.; manganese) and lanthanides, respectively. However, doping CaZnOS needs for stringent control of synthetic conditions. CaZnOS crystals are typically formed in a narrow temperature window (1370K–1520K). At elevated temperatures, CaZnOS experiences a weight loss because of melting and decomposition of the eutectic[10]. Due to limited reactivity of lanthanide precursors at moderate reaction temperatures, the amount of lanthanide dopants that can enter the CaZnOS host lattice are typically small (< 2%).

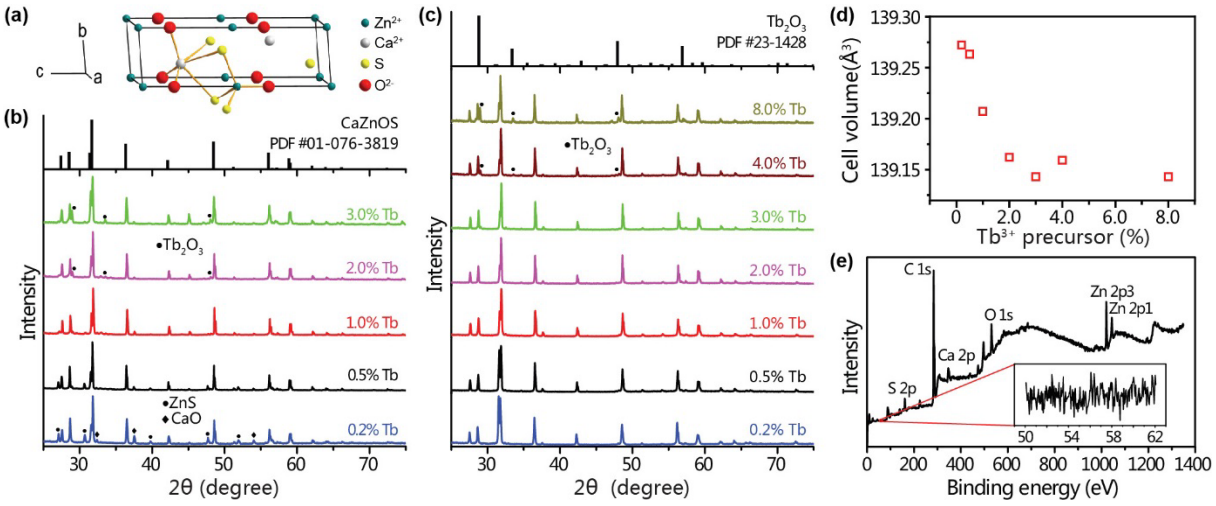

Figure 1. (a) Schematic presentaton of crystal structure of CaZnOS. (b,c) XRD patterns of Tb^{3+}-doped CaZnOS synthesized without and with the assistance of $LiNO_3$, respectivley. (d) Cell

volumes of CaZnOS:Tb^{3+} derived from the XRD patterns in c. (e) XPS spectrum of CaZnOS:Tb (3%) after purification with water for three times.

In order to facilitate incorporation of lanthanide dopants into the lattice of CaZnOS crystals, lithium nitrate was introduced as a fluxing agent to enhance the reactivity of the precursors. In addition, lanthanide fluorides were used to replace lanthanide chlorides and oxides as lanthanide precursors in the synthesis. The use of lanthanide fluorides avoids the problems associated with hygroscopic effect and change of valence state, which are typically encountered by chloride and oxide precursors. Notably, fluoride was also found to promote chemical reaction between the starting materials (vide infra).

We first assessed the effect of lithium nitrate on prompting the doping process by using Tb^{3+} as a model dopant. The crystals were prepared by annealing $CaCO_3$, ZnS, and TbF_3 at 1373 K for 2 hr under nitrogen atmosphere. All samples were first characterized by X-ray power diffraction (**Figure 1 b and c**). Without the use of $LiNO_3$, unreacted ZnS and CaO impurities were clearly seen at a low Tb^{3+} concentration (0.2%). The unreacted impurities gradually disappeared with increasing TbF_3 content, suggesting that fluoride promotes chemical reactions between ZnS and CaO. However, Tb_2O_3 impurities were formed at a concentration of Tb^{3+} precursor as low as 1%, indicating that Tb^{3+} ions were not effectively incorporated into the CaZnOS lattice. When lithium nitrate was involved in the synthesis (6 mol% with respect to the total amount of Ca^{2+} and Tb^{3+}), the formation of doped CaZnOS is greatly improved. No noticeable impurity phases were detected in the Tb^{3+} concentration range of 0.2–3% under the same experimental conditions (**Figure 1c**).

Figure 1d shows structural analysis of the Tb^{3+}-doped CaZnOS crystals by Rietveld refinement using total pattern analysis solution (TOPAS) **(Figure S1a).** The results revealed a steady decrease of cell volume with increasing the dopant concentration of Tb^{3+} to 3 %, supporting successful substitution of Tb^{3+} dopant for larger host Ca^{2+} ions (0.92 versus 1.00 Å). We found that the dopant concentration was unlikely to be further increased by using larger amount of Tb^{3+} precursor, even elevated content of lithium nitride was used **(Figure S1b).** X-ray photoelectron spectroscopy (XPS) spectrum obtained from CaZnOS:Tb (3%) revealed the presence of Tb 3d peaks **(Figure S1c)**, while the Li 1s peak is absent (**Figure 1e**)[11]. The results indicate that lithium nitrate plays the role of a fluxing agent rather than a co-dopant.

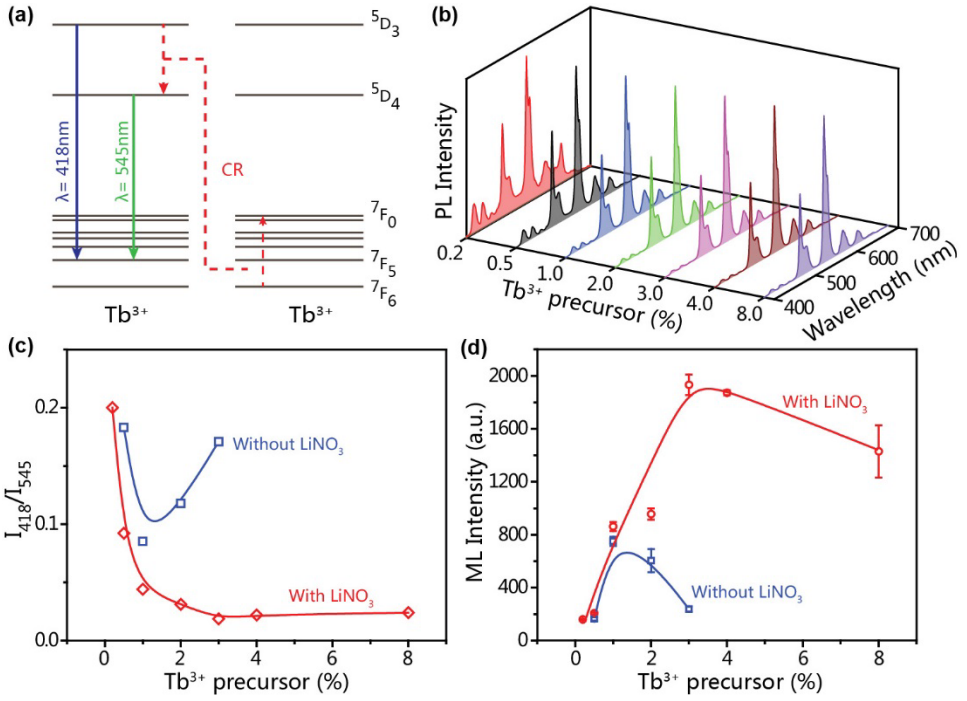

Figure 2. (a) Simplified energy-level diagram showing cross-relaxation between Tb^{3+} ions. (b) PL spectra the Tb^{3+}-doped CaZnOS under excitation of 285nm. The spectra were normalized at 545 nm. (c) Comparison of I_{418} ($^5D_3 \rightarrow {}^7F_5$) to I_{545} ($^5D_4 \rightarrow {}^7F_5$) emisison intensity ratio for CaZnOS:Tb^{3+} prepared without and with the assistance of $LiNO_3$. (d) Comparison of PL (阳阳：change to PL) intensity for CaZnOS:Tb^{3+} prepared without and with the assistance of $LiNO_3$.

The effective incorporation of Tb^{3+} into the host lattice was validated by spectroscopic inversitgations. Due to $^5D_3 + {}^7F_6 \rightarrow {}^5D_4 + {}^7F_0$ cross-relaxation between neighbouring Tb^{3+} dopants (**Figure 2a**), the emission peaks corresponding to $^5D_3 \rightarrow {}^7F_J$ tranistions are attenuated with respect to those originating from $^5D_4 \rightarrow {}^7F_J$ transitions as dopant concnetration of Tb^{3+} increases[12]. The photoluminescence spectra in **Figure 2b** show a steady decrease in emission intensity ratio of I_{418} ($^5D_3 \rightarrow {}^7F_5$) and I_{545} ($^5D_4 \rightarrow {}^7F_5$) for samples prepared in the presence of increasing amount of Tb^{3+} precursors from 0.2 to 3%. Further attenuation of emission from $^5D_3$ state was not observed on continous increase in concentration of Tb^{3+} precursors. The results suggest that no more Tb^{3+} dopants could enter the host lattice, in good aggreement with the XRD charaterization of the samples. Notably, higher I_{418} / I_{545} ratios were detected for samples prepared in the absence of $LiNO_3$ (**Figure 2c and Figure S2**), revealing that the actual concentration of dopants in the host lattice is relatively low. The effect of $LiNO_3$ on promoting the incorperation of lanthanide ions into the CaZnOS lattice is further supported by the enhanced integral emission intensity (**Figure 2d**).

We next invesitigated ML properties of the Tb^{3+}-doped CaZnOS crystals. CaZnOS is a wide-bandgap piezoelectric semiconductor (d_{33}=38 pm V^{-1}, E_g=3.88eV)[13]. When external force is applied, the noncentral symmetry enables the generation of piezoelectric polarization charges within the CaZnOS, which produces inner crystal piezo potential and tilts the conduction and valence band[2]. As a result, the trapped electron of CaZnOS associated with intrinsic vacancies V_O^{2+}, V_{ZnO}^{2+}, and V_{CaZnOS}^{2+} is ejected to the acceptor state induced by neutral oxygen vacany V_O^0. Subsequent recombination between detrapped electron and hole levels occurs and the released energy is transfered to the dopant ions (**Figure 3a**) [14].

ML spectrum of the Tb^{3+}-doped CaZnOS show characteristic emisison peaks spanning violet to red spectral region due to electronic tranistions from both the $^5D_3$ and $^5D_4$ states of Tb^{3+} (**inset of Figure 3a**). However, intrinsic defect emission peak is located at ~520 nm, and the corresponding energy is insufficient to populate the $^5D_3$ state of Tb^{3+}. Thus, we speculate that excitation of Tb^{3+} dopants was estabished by upconversion through successive energy transfer. Our results also showed that samples prepared with 3% of Tb^{3+} precursor displayed the strongest ML intensity (**Figure S3**). The observations were ascribed to the highest Tb^{3+} content in the host lattice that extracted the most amount of energy from the host. Thus, effective lanthanide doping through the use of lithium nitrate as a flux agent is important for boosting ML intensities. Notably, the 3% Tb^{3+}-doped CaZnOS renders comparative ML intensity to that of the well-established CaZnOS:Mn **(Figure S4)**, demonstrating high efficiency of the lanthanide-doped CaZnOS for ML.

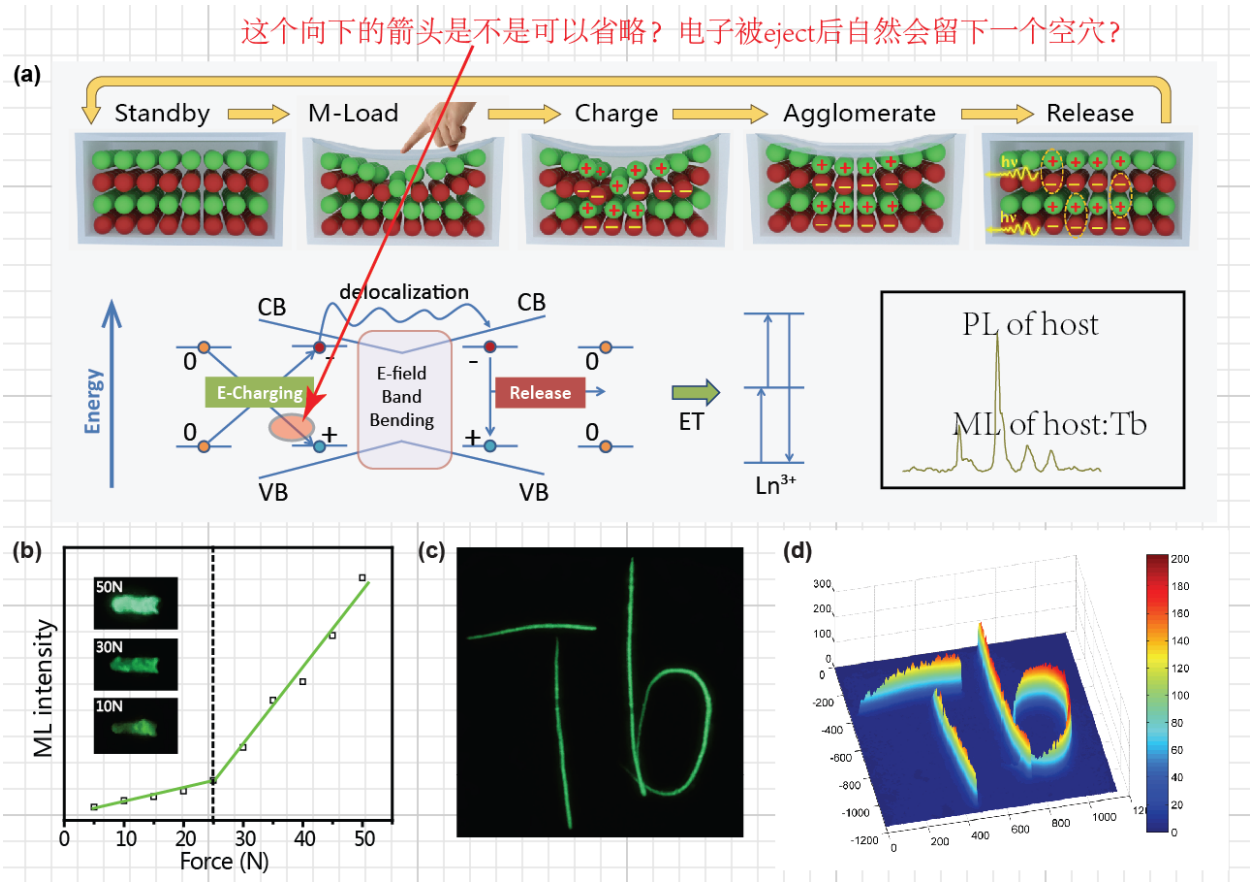

Figure 3. (a) Proposed ML mechanism in the lanthanide-doped CaZnOS crystals. The overall energy diagram for electronic-transition undergoes within neutral charge environment. The Standby mode means a materials without any mechano-stimuli. The M-load mode is for mechano-stimuli applying on the host. Charge mode stands for defects induced spatial charge separations. The Agglomerate mode is the charged defect undergoes an agglomeration within the host. The Release represents the final energy releases in terms of photon-emissions. (The VB=valence band, CB=conduction band, E-field=electric field, E-Charging=E-field induced charge-separation, ET=energy transfer, Ln^{3+}=trivalent lanthnide ion. Orange balls=neutral defect centers, red balls=electrons, and blue balls=holes) (b) Integral ML intensity versus applied force for the CaZnOS:Tb (3%) crystal. Inset: ML images of the sample under forces of 10N, 30N, and 50N. (c) Visualization of handwriting trajectory through long time exposure ML imaging. (d) The distribution of relative ML intensity extracted from ML image in (c) accroding to the gray scale value.

The ML performace of the Tb^{3+}-doped CaZnOS crystals under varying amount of forces were also assessed. In general, the ML intensity increases with increasing the applied force (**Figure 4a**). However, two distinct regions can be clearly identified for the stress-depedent ML behavior (**Figure 4b**), suggesting a variation of ML mechanism as the applied force increases.

The ML at relatively low strength of force (< 25N) is ascribed to the triboelectric effect in which frictional contact between PET and ML crystals induce tribocharge at the contact surface[15]. The electric potential associated with the surface charges is responsible for the excitation of electrons. With increasing of applied forces, distoration of the CaZnOS host appears and causes dramatic change in piezoelectric potential of the host, thereby leading to rapid growth of the ML intensity. The same ML depedence on applied forces was also observed for Mn^{2+}-doped CaZnOS **(Figure S5)**, indicating generality of the underlying mechanism.

The CaZnOS:Tb crystals release photons fast and show no afterglow emissions. This feature together with positive correlation between ML intensity and applied force is useful for stress sensing. To illustrate this property, we recorded ML signals from a thin film comprising the ML crystals under single-point dynamic pressure of a ball-point pen (ball diameter: 0.7 mm). A digital camera with a long-duration shutter speed was used for capturing 2D distribution of the emissions. **Figure 4c** presents visualization of a 2D planner presure map by capturing a handwritten letter “Tb”. By extracting the gray scale of the ML photograph, the relative ML intensity were derived and shown in **Figure 4d**. The intensity profile clearly reveals varation of relative intensity between different points on the trajectory, demonstrating capability of this platform for acquiring detailed pressure information.

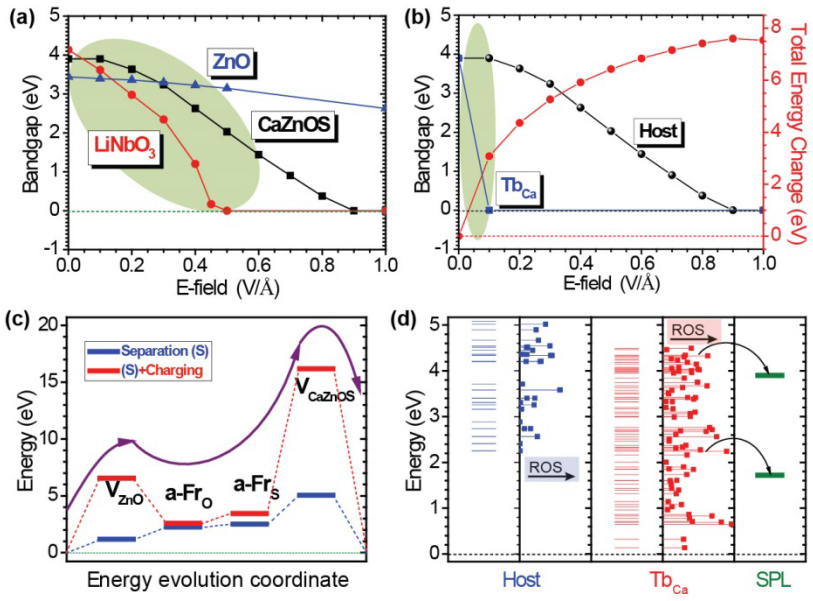

Figure 4. (a) Comparison of bandgap variations for $LiNbO_3$, CaZnOS and ZnO lattices as a function of external electric field (E-field) applied along the *c*-axis. The green shaded area highlights the region of high sensitivity to E-field for the three host systems. (b) The variation trends of optical bandgap and system energy with applied E-field for CaZnOS. The host bandgap after formation of Tb_{Ca} is also shown. The green shaded area highlights the region of high sensitivity to E-field. (c) Free energy variation pathway along different native complex defects in undoped CaZnOS lattice. The purple line is treated as continuous smearing that potentially considers another more specific defect complex to shape the energy evolutions within this trend. (d) Excited state calculations of CaZnOS host, Tb_{Ca}, and the single particle levels (SPLs) of Tb_{Ca}. ROS stands for relative oscillator strength.

To gain insight into the mechanism responsible for the high ML performance, we performed DFT calculations of the lattice matrix under small electric-field strength (E-field). Benchmark of bandgap variation indicates that CaZnOS crystal displays a sensitive response character to the E-field, similar to $LiNbO_3$ that is known as one of the most efficient piezoelectric materials[16] (**Figure 4a**). Furthermore, the bandgap evidently decreased even with very small E-field strength due to the Tb_{Ca} (**Figure 4b**). This implies that higher concentrations of electrons can be excited onto delocalized conducting state for different forms of transitions near the dopants. As we summarized, the magnitude of total energy change within small E-field support the formation and spatial-charge-separation of ZnO-vacancy (V_{ZnO}), which is a kind of

Schottky-like intrinsic defect complex (**Figure 4c**). This type of intrinsic host defect is responsible for the native 500-520 nm host luminescence. Excited state energy level calculation demonstrates that the Tb_{Ca} lowers the adsorption edges and increases electronic populations in the excited states owing to the higher relative oscillator strengths (ROS) in comparison with the pristine host matrix (**Figure 4d**). From the ground state single particle level (SPL) calculations, we found that the Tb_{Ca} results in the formation of two defect levels that are 1.72 eV and 3.71 eV above the top of valence band, respectively. The long-lifetime SPLs display slightly lower positions relative to that of the dopant levels, and are able to trap the excited electrons for extending energy transfer steps within the host. In comparison with the undoped host, the relatively high oscillator strength of Tb_{Ca} indicates enhanced inter-level transitions instead of de-excitations backward to ground state, which facilitate tunneling to the SPLs[17] (**Figure 4d**). Therefore, CaZnOS:Tb can be considered as an ML system involving substantial energy transfer interactions.

The Li-assisted annealing protocol is equally effective for incorperation of other types of lanthanide activators into CaZnOS crystals. XRD measurements reveal single phase of the products at a dopant concentration of 2% **(Figure S6).** Althought further increase dopant concentration results in minor impurity phase for heavy lanthanides, continous growth of the emission intenstities were typically detected (**Figure S7**). Thus, we can conclude that more than 2% of lanthanide dopants can be generally incorporated into CaZnOS host by using our synthetic protocol. Owing to the relatively high dopant concentration, these CaZnOS crystals all display intense ML, spanning a broad spectral range from green (CaZnOS:Pr, CaZnOS:Ho, and CaZnOS:Er), to yellow (CaZnOS:Dy), red (CaZnOS:Sm and CaZnOS:Eu), and near-infrared (CaZnOS:Tm, CaZnOS:Nd, and CaZnOS:Yb) (**Figure 5**).

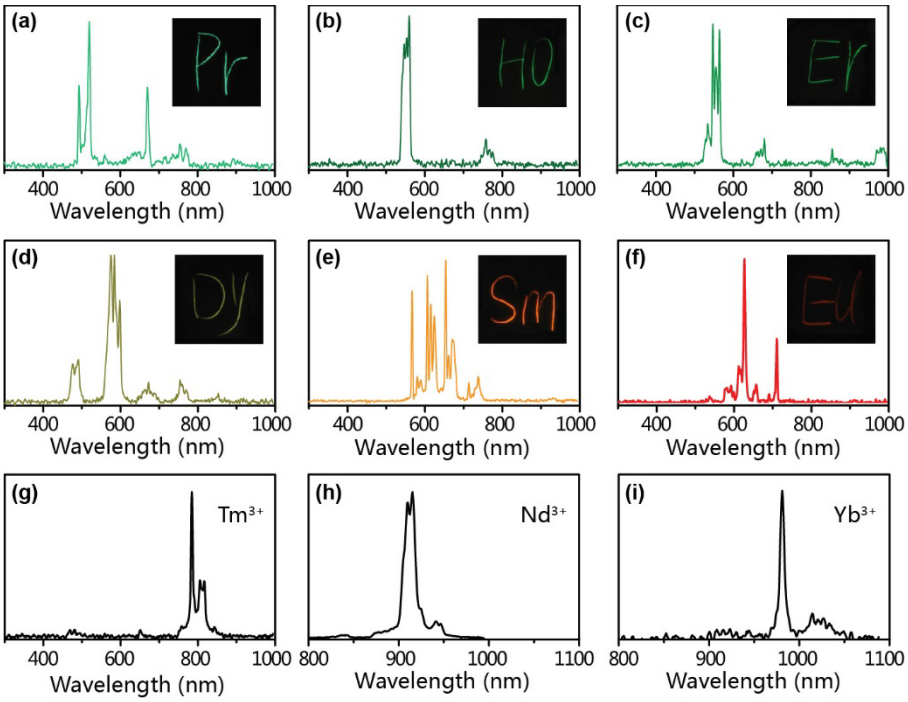

Figure 5. ML spectra of CaZnOS doped with (a) Pr^{3+}, (b) Ho^{3+}, (c) Er^{3+}, (d) Dy^{3+}, (e) Sm^{3+}, (f) Er^{3+}, (g) Tm^{3+}, (h) Nd^{3+}, and (i) Yb^{3+}, respectively. Inset: photographs of the corresponding samples under single-point dynamic pressure of a ball-point pen.

In a further set of experiments, we demonstrated that ML color can be alternatively manipulated by uisng mixtures of differently doped CaZnOS crystals. The newly developed green emitting CaZnOS:Tb crystals (denoted as "G") were mixed with classical red emitting CaZnOS:Mn (denoted as "R") for color tuning. Owing to their comparative emission intensity, the mixture displays dual emissions from both the G and R components. By adjusting the weight ratio of the G and R components, the relative intensity ratio of the dual emissions can be precisely manipulated (**Figure 6a**). The adjustable balance of emission intensities allows precise manipulation of ML color from green to red (**Figure 6b**).

The availability of bright multicolor ML offers promising opportunities for anti-counterfeiting and security applications[18]. ML materials that are excited by mechanical force are advantageous over photoluminescent materials for such applications as they do not require

excitation sources such as ultraviolet lamps and near-infrared lasers. As a proof-of-concept, we prepared an anti-countifeiting pattern composed of ML strip arrays. Each ML strip is tagged with a particular type of ML material. By writting across the strips with a ball-point pen, a sequence of color segments corresponding to the encrypted information can be extracted. Througth control of permutations of the ML materials and/or sizes of the strips, distinct covert information can be encrypted as illustrated in **Figure 6c and d**. Notably, the lanthanide-doped CaZnOS crystals preserve excellent photoluminescence properties of the lanthanide ions such as tunable photon upconversion **(Figure S8)**, which imparts additional modilities to the platfrom for extra high-level security protection[19].

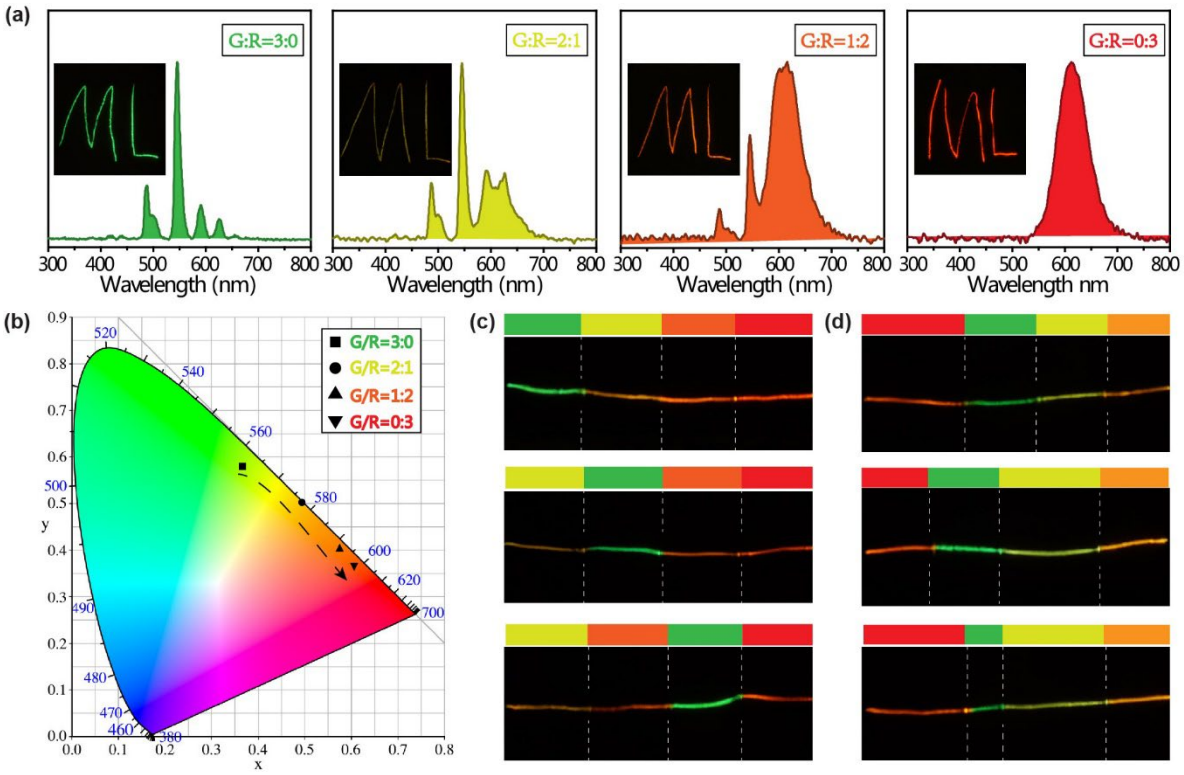

Figure 6. (a) ML multicolor tuning by mixing CaZnOS:Tb (denoted as 'G') and CaZnOS:Mn (denoted as 'R') in different ratios. (b) Commission International de l'Eclairage (CIE) chromaticity coordinates of the multicolor emissions from the composite samples in a. (c,d) Photographs of anti-countifeiting patterns encoded with ML strips of varying colors sequence and strip width, respectively.

Conclusions:

In summary, we have successfully incorperated a wide collection of lanthanide ions into CaZnOS crystals and achieved tunable ML spanning the full sepctrum from violet to near infrared. Particularly, we have demonstrated for the first time ML in Tb^{3+}, Eu^{3+}, Tm^{3+}, and Yb^{3+} ions. The newly developed ML systems show comparable ML performance to that of the well-established CaZnOS:Mn. By mixing Mn^{2+}- and Tb^{3+}-activated CaZnOS at prescribed mass ratios, we have achieved fine-tuning of ML colors from green to red with high brightness. The multicolor ML materails are promising for constructing optically encoded aniti-counterfeiting patterns. Our study validates the generality of using common photoluminescent dopants to modulate ML processes. In addition, the lithium-assisted synthetic protocol could be extended for efective doping of other types of functional materials, thereby enabling an improved control over materials properties[3].

Experimental Section

Detailed experimental procedures are reported in the Supporting Information.

Supporting Information

Supporting Information is available from the Wiley Online Library or from the author.

Acknowledgements

This work was supported by the National Natural Science Foundation of China (No. 21773200), the Research Grants Council of Hong Kong (CityU 11204717, Project Code: 9042485), and City University of Hong Kong (Project 9667171). D.P. acknowledges the Natural Science Foundation

of China (Nos. 51502018 and 61875136), Shenzhen Fundamental Research Project (No. 000102), and Scientific Research Starting Foundation for the Youth Scholars of Shenzhen University (No. 000127).

Received: ((will be filled in by the editorial staff))
Revised: ((will be filled in by the editorial staff))
Published online: ((will be filled in by the editorial staff))

References

[1] a) S. M. Jeong, S. Song, H. J. Seo, W. M. Choi, S. H. Hwang, S. G. Lee, S. K. Lim, *Adv. Sustainable Syst.* **2017**, 1, 1700126; b) D. Tu, D. F. Peng, C. N. Xu, A. Yoshida,. *J. Ceramic. Soc. Jpn.* **2016**, 124, P6-1; c) S. M. Jeong, S. Song, H. Kim, K. Joo, H. Takezoe, *Adv. Funct. Mater.* **2016**, 26, 4848; d) J. Zhang, L. Bao, H. Q. Lou, J. Deng, A. Chen, Y. Z. Hu, Z. Zhang, X. M. Sun, H. S. Peng, *J. Mater. Chem. C* **2017**, 5, 8027; e) X. S. Wang, C. N. Xu, H. Yamada, K. Nishikubo, X. G. Zheng, *Adv. Mater.* **2005**, 17, 1254.

[2] a) X. Wang, H. Zhang, R. Yu, L. Dong, D. Peng, A. Zhang, Y. Zhang, H. Liu, C. Pan, Z. L. Wang, *Adv. Mater.* **2015**, 27, 2324; b) B. P. Chandra, V. K. Chandra, S. K. Mahobia, P. Jha, R. Tiwari, B. Haldar, *Sens. actuators. A Phys.* **2012**, 173, 9; c) C. N. Xu, T. W., M. Akiyama, X. G. Zheng, *Appl. Phys. Lett.* **1999**, 74, 1236; d) S. M. Jeong, S. Song, K. Joo, J. Kim, S. H. Hwang, J. Jeong, H. Kim, Hyunmin. *Energy Environ. Sci.* **2014**, 7, 3338.

[3] a) P. T. Diallo, P. Boutinud, R. Mahiou, J. C. Cousseins, *Phys. Status Solidi A* **1997**, 160, 255; b) Z. Xie, T. Y., J. Chen, E. Ubba, L. Wang, Z. Mao, T. Su, Y. Zhang, M. P. Aldred, Z. Chi, *Chem. Sci.* **2018**, 9, 5787; c) H. W. Zhang, H. Yamada, N. Terasaki, C. N. Xu, *J. Electron. Mater.* **2008**, 155, J55; d) H. W. Zhang, H. Yamada, N. Terasaki, C. N. Xu, *Appl. Phys. Lett.* **2007**, 91, 081905; e) J. C. Zhang, C. N. Xu., Y. Z. Long, *Opt. Express* **2013**, 21, 13699; f) J. Botterman, K. V. Eeckhout., I. D. Baere, D. Poelman, P. F. Smet, *Acta Mater.* **2012**, 60, 5494.

[4] a) J. C. Zhang, Y. Z. L., X. Yan, X. V. Wang, F. Wang, *Chem. Mater.* **2016**, 28, 4052; b) D. Tu, C. N. X., Y. Fujio, A. Yoshida, *J. Phys. D: Appl. Phys.* **2015**, 48, 475105; c) Y. Zhang, G. Gao, H. L. Chan, J. Dai, Y. Wang, J. Hao, *Adv. Mater.* **2012**, 24, 1729; d) M. C. Wong, L. Chen, G. Bai, L. B. Huang, J. Hao, *Adv. Mater.* **2017**, 29; e) D. Tu, C. N. X., Y. Fujio, *J. Adv Dielectr.* **2014**, 04, 1450017.

[5] a) B. L. Huang, M. Z. Sun, D. F. Peng, *Nano Energy* **2018**, 47, 150; b) V. K. Chandra, B. P. Chandra, P. Jha,. *Appl. Phys. Lett.* **2013**, 102, 241105; c) B. L. Huang, *Phys. Chem. Chem. Phys.* **2016,** 18, 25946.

[6] Z. J. Zhang, A. Feng, X. Y.Chen, J. T. Zhao, *J. Appl. Phys.* **2013,** 114, 213518.

[7] J. C. Zhang, L. Z. Zhao, Y. Z. Long, H. D. Zhang, B. Sun, W. P. Han, X. Yan, X. S. Wang, *Chem. Mater.* **2015**, 27, 7481.

[8] J.-C. G. Bunzli, K.-L. Wong, *J.* Rare Earths **2018,** 36, 1.

[9] a) H. L. Zhang, D. Peng, W. Wang, L. Dong, C. F. Pan, *J. Phys. Chem. C* **2015**, 119, 28136; b) L. J. Li, L. Wondraczek., L. Li, Y. Zhang, Y. Zhu, M. Y. Peng, C. B. Mao, *ACS Appl. Mater. Interfaces* **2018**, 10, 14509; c) W. Wang, D. F. Peng, H. L. Zhang, X. H. Yang, C. F. Pan, *Opt. Commun*. **2017**, 395, 24.

[10] R. I. Gulyaeva, E. N. Selivanov, A. D. Vershinin, V. M. Chumarev, *Inorg. Mater.* **2006**, 42, 897.

[11] L. Suo, Y. S. Hu, H. Li, M. Armand, L. Chen, *Nat. Commun.* **2013**, 4, 1481.
[12] B. Chen, D. Peng, X. Chen, X. Qiao, X. Fan, F.Wang, *Angew. Chem. Int. Ed. Engl.* **2015**, 54, 12788.
[13] T. Sambrook, C. F. Smura,, and S. J. Clarke, *Inorg. Chem.* **2017**, 46, 2517.
[14] a) C. Pan, J. C. Zhang, M. Zhang, X. Yan, Y. Z. Long, X. S. Wang, *Appl. Phys. Lett.* **2017**, 110, 233904; b) J. J. Joos, K. Lejaeghere,, K. Korthout, A. Feng, D. Poelman, P. F. Smet, *Phys. Chem. Chem. Phys.* **2017**, 19, 9075; c) B. P. Chandra, V. K. C Chandra, P. Jha, *Physica B Condens Matter.* **2015**, 461, 38.
[15] a) X. Y. Wei, X. Wang, S. Y. Kuang, L. Su, H.Y. Li, Y. Wang, C. Pan, Z. L. Wang, G. Zhu. *Adv. Mater.* **2016, 28**, 6656; b) H. Matsui, C. N. Xu, Y. Liu, H. Tateyama, *Phys. Rev. B* **2004**, 69, 235109.
[16] D. Tu, C. N. Xu, A. Yoshida, M. Fujihala, J. Hirotsu, X. G. Zheng, *Adv. Mater.* **2017**, 29, 1606914.
[17] Z. Pan, Y. Y. Lu, F. Liu, *Nat. Mater.* **2011**, 11, 58.
[18] a) J. C. Zhang, C. Pan, Y. F. Zhu, L. Z. Zhao, H. W. He, X. Liu, J. Qiu, *Adv. Mater.* **2018**, 1804644; b)H. Hu, Q. W. Chen., J. Tang, X. Y. Hu, X. H. Zhou, *J. Mater. Chem*. **2012**, 22, 11048.
[19] T. Sun, B. Xu, B. Chen, X. Chen, M. Li, P. Shi, F. Wang, *Nanoscale* **2017**, 9, 2701.